Surface Science 606 (2012) 598–604

Contents lists available at SciVerse ScienceDirect

Surface Science

journal homepage: www.elsevier.com/locate/susc

Structural and electronic properties of cobalt carbide Co_2C and its surface stability: Density functional theory study

Yong-Hui Zhao, Hai-Yan Su, Keju Sun, Jinxun Liu, Wei-Xue Li *

State Key Laboratory of Catalysis, Dalian Institute of Chemical Physics, Chinese Academy of Sciences, Dalian 116023, China

ARTICLE INFO

Article history:
Received 2 September 2011
Accepted 18 November 2011
Available online 3 December 2011

Keywords:
Cobalt carbide
Surface structure
Stability
Density functional theory

ABSTRACT

Density functional theory calculations have been performed to investigate the structural and electronic properties of bulk Co_2C and the stability of low index Co_2C surfaces. We found that the formation of Co_2C is exothermic with the formation energy of −0.81 eV/Co_2C with respect to Co under the presence of syngas (mixture of CO and H_2). While formed Co_2C can be decomposed further to metal Co and graphite carbon with modest energy gain of 0.37 eV/Co_2C. This suggests that Co_2C is only metastable in Fischer–Tropsch synthesis, which agrees well with experimental findings. The density of states (DOSs) reveals that the Co_2C is paramagnetic and strong metallic-like. The difference of charge density analysis indicates that the bond of Co_2C is of the mixtures of metallic, covalent, and ionic properties. A variety of low index Co_2C surfaces with different terminations are studied. We find that the surface energy of low index stoichiometric Co_2C highly relies on the surface area, the number of coordination of surface atoms and the surface dipole, with the decreased stability order of (101) > (011) > (010) > (110) > (100) > (001) = (111). Our results indicate that under Co-poor condition, the formation of non − stoichiometric surface (011) and (111) without terminated cobalt is energetically more favorable, while under Co-rich condition the formation of non − stoichiometric (111) surface with cobalt overlayer are preferential.

© 2011 Elsevier B.V. All rights reserved.

1. Introduction

Transition metal carbides (TMCs), typically including all 3 d elements and 4 d/5 d elements of groups 3–6 early transition metals, possess unique physical and chemical properties [1–7]. For example, TMC compounds often demonstrate extreme hardness and brittleness, high melting points and electrical as well as thermal conductivities [8], which make them attractive in technological applications as cutting tools [1] and hard-coating materials [9]. In addition, since Levy and Boudart's pioneering work regarding the Pt-like properties of tungsten carbides [10], the catalytic properties of TMCs have been the subject of many research fields of catalysis and surface science. It has been reported that the TMCs exhibit excellent catalytic performance in hydrogenation [11–14], dehydrogenation [15], hydrogenolysis [16,17] and Fischer–Tropsch synthesis (FTS) [18–22] etc., approaching or surpassing those of precious Pt-group metals [2,3,5]. Excellent reviews on the various properties of TMCs can be found in Refs. [2–5,8,23].

Despite numerous theoretical studies have been done about the catalytic activity of cobalt, iron and iron carbide in Fischer–Tropsch synthesis (FTS)[24–43], relative little attention has been paid to the cobalt carbides, which has also in connection with the Fischer–Tropsch synthesis (FTS). The formation of carbide, especially Co_2C, is often referred to as a sign of deactivation and the active components on cobalt catalysts are usually considered to remain in metallic states during FTS [44,45]. For example, Ducreux et al. [45] observed the formation of Co_2C on a supported cobalt catalyst during FTS by in-situ XRD, which was related with the deactivation process of the sample. These observations have been supported by Tihay et al. [46,47], who reported that when an Fe–Co-based catalyst is used for FTS, metallic Co particles on the surface are partly transformed to Co_2C, as revealed by high-resolution transmission electron microscopy (HRTEM). Based on density functional theoretical (DFT) calculation, Cheng et al. [48] proposed that the deactivation came from the high methane selectivity of the Co_2C. It was also found [45–47,49,50] that those cobalt carbides are unstable, and decomposed to metallic cobalt and polymeric carbon easily, so that they have rarely been observed by ex-situ techniques. In addition, Co_2C was also common identified species in the production of H_2 from the steam reforming of alcohols [51] as well as in the formation of higher alcohol synthesis [52–54]. Recently, Ding and co-workers [55] showed that mixed linear α-alcohols (C_1–C_{18}) can be directly synthesized from syngas over the La-doped Co catalysts under mild conditions and that the selectivity towards alcohols was substantially improved. They found that La_2O_3 can promote the formation of cobalt carbides (Co_2C), which were postulated to play an important role in the syntheses of the mixed linear α-alcohols.

In this paper, we present a first principle study of the structural and electronic properties as well as the stability of Co_2C bulk and a variety of the low-index surfaces. The achieved insights are important in

* Corresponding author. Tel.: +86 411 84379996; fax: +86 411 84379996.
E-mail address: wxli@dicp.ac.cn (W.-X. Li).

0039-6028/$ – see front matter © 2011 Elsevier B.V. All rights reserved.
doi:10.1016/j.susc.2011.11.025

further understanding the relationship between structure and catalytic properties of Co_2C in FT synthesis and alcohols formation etc., which has not been addressed in literatures so far. In this context, we note that though we focus on the cobalt carbide in the present work, the co-existence of the metallic cobalt with the presence of the interstitial carbon or even the formation of the surface carbide under reaction conditions could not be excluded, as indicated in the recent theoretical study on Pd [56,57] and Ni [58]. Further theoretical studies of the interstitial carbon in the cobalt catalysts as well as the effects on the selectivity are important but not addressed in the present work. The paper is organized as follows. The theoretical section including theoretical approaches, computational details and crystal structure is summarized in Section 2. The results and discussion are presented in Section 3. Finally, the conclusions are summarized.

2. Computational details

Calculations were done with Vienna Ab-initio Simulation Package (VASP) [59,60], which performs an iterative solution of the Kohn–Sham equations in a plane wave basis set. The exchange correlation energy was calculated within the generalized gradient approximation (GGA) using the form of the functional proposed by Perdew and Wang [61,62], which referred to as Perdew–Wang 91 (PW91). The electron–ion interactions for C, and Co were described by the projector-augmented wave (PAW) method developed by Blöchl [63,64]. The kinetic energy cut-off of 400 eV was used for the plane wave basis set. It should be noteworthy that spin polarization was found to be essential in order to appropriately describe a system including magnetic properties of Co and was therefore included in all the calculations.

As seen from Fig. 1, Co_2C has an orthorhombic structure (space group Pmnn), with two formula units per unit cell, in which all cobalt atoms and carbon atoms are equivalent. The carbon atoms occupy at the octahedral interstitial sites of Co, and C atoms and Co atoms are 6-coordinated and 3-coordinated respectively.

For the slab, geometry optimizations were performed by minimizing the energy to within 10^{-4} eV and inter-atomic forces were performed by minimizing to within 0.02 eV/Å. Monkhorst–Pack mesh [65] for k-point sampling was used in all calculations, i.e., $(10\times8\times8)$ for the Co_2C bulk, $(6\times6\times1)$, $(8\times6\times1)$, $(8\times6\times1)$, $(4\times6\times1)$, $(8\times4\times1)$, $(6\times4\times1)$ and $(6\times6\times1)$ k-point meshes for the seven low index stoichiometric (100), (001), (010), (101), (011), (110) and (111) surfaces, respectively. The k-point meshes for different surfaces are selected in such a way that the sampling density in momentum space is approximately similar to minimize the possible numeric error. A large vacuum region of 15 Å was used between two neighbor slabs to prevent interactions between periodic slabs. The top and bottom two layers of the surfaces are allowed to relax, while the remained are fixed in their bulk truncated positions. Further relaxation of the deeper layers was found to change the surface energies less than 1%, which indicates a sufficient convergence of the presence set up.

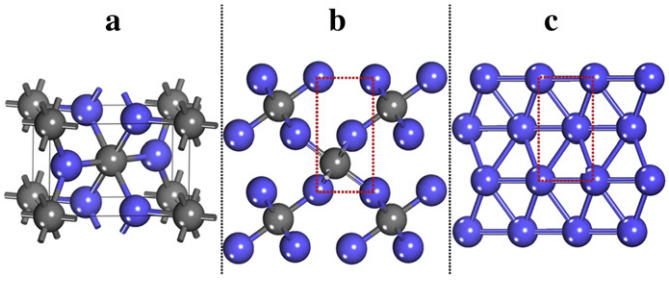

Fig. 1. (a) shows the unit cell of Co_2C. (b) was the same unit cell stack of bulk Co_2C as in (a) but from 001 view. (c) shows the stack of bulk hcp type Co. Dashed frame in (b) and (c) show the ABAB…stacking of Co. The grey and bule balls represent C and Co atoms, respectively.

To study the surface structures and stability of Co_2C, we selected seven low index (100), (001), (010), (101), (011), (110) and (111) surfaces in a $p(1\times1)$ unit cell with either stoichiometric or non-stoichiometric termination. The surface energy for stoichiometric surfaces is calculated by

$$\gamma = \left(E_{stoic}^{slab} - NE_{Co_2C}^{bulk}\right)/2A, \tag{1}$$

Here, E_{stoic}^{slab} is the total energy of the stoichiometric slab, N is the number of Co_2C units in the slab, $E_{Co_2C}^{bulk}$ is the bulk total energy per Co_2C formula, A is the corresponding (1×1) surface area, and the factor 1/2 corresponding to the symmetric terminations. The lower the surface energy, the more stable the surface. Surfaces were represented by slabs thick range from 10.07 to 28.23 Å. To calculate the surface energy calculations accurately, the thickness of the slab was increased gradually until the difference of the total energy between two consecutive slabs is equal to the total energy of the cobalt carbide bulk for all the surfaces considered.

It should be noted that it is impossible to calculate surface free energy of the non-stoichiometric surfaces without taking into account of the thermodynamics under the reaction conditions. For instance, those present in true carburizing environments will undoubtedly alter the situation, and produce surfaces with non-stoichiometric compositions. To explore the relative stability of the non-stoichiometric surfaces, we introduce the so-called differential adsorption energy E_{diff}^{stoic}, E_{diff}^{extra} by removing terminated Co atoms or adding extra Co atoms with respect to stoichiometric surface:

$$E_{diff}^{stoic} = \left(E_{non-stoic}^{slab} - E_{stoic}^{slab} + N_{ex}E_{Co}^{bulk}\right)/N_{ex}, \tag{2}$$

$$E_{diff}^{extra} = \left(E_{non-stoic}^{slab} - E_{stoic}^{slab} - N_{ex}E_{Co}^{bulk}\right)/N_{ex}, \tag{3}$$

where $E_{non-stoic}^{slab}$ is the total energy of the non-stoichiometric surfaces, and N_{ex} is the number of removing or adding Co atoms with respect to stoichiometric surfaces, and E_{Co}^{bulk} is total energy of the bulk hcp Co metal. In this convention, negative E_{diff}^{stoic} and E_{diff}^{extra} indicates that the formed Co-poor and Co-rich non-stoichiometric surfaces are energetically favorable with respect to the stoichiometric ones. Especially, the negative E_{diff}^{stoic} means that the Co atoms of the surface would tend to aggregate and form small Co nanoparticles.

3. Results and discussion

3.1. Bulk properties

We first optimized the lattice constants of Co_2C using the experimental lattice constants as initial values [66]. As listed in Table 1, there is a quite good agreement between our results ($a=2.877$ Å, $b=4.386$ Å, and $c=4.354$ Å) and previous calculations ($a=2.921$ Å, $b=4.479$ Å, and $c=4.411$ Å) [48], which are both in line with the experimental ones ($a=2.897$ Å, $b=4.446$ Å, and $c=4.371$ Å) [66]. The differences between our calculated parameters and the experimental ones as well as the previously theoretical studies are less than 1%, which fall well in typical error bar reported in literatures. It can be

Table 1
Computed lattice constant (Å) and calculated formation energy of Co_2C (ΔH_{Co_2C}, eV/Co_2C) with respect to CO and H_2. The previous calculation (Ref [48]) and experimental results (Ref. [66]) are given for reference.

	a	b	c	ΔH_{Co_2C} (eV/Co_2C)[n]
Present	2.877	4.386	4.354	−0.81
Ref [48]	2.921	4.479	4.411	–
Exp. (Ref. [66])	2.897	4.446	4.371	–

[n] $\Delta H_{Co_2C} = \mu_{Co_2C}^{bulk} + \mu_{H_2O} - \mu_{CO} - \mu_{H_2} - 2\mu_{Co}^{bulk}$

seen from Fig. 1 that each cobalt atom in the (001) plane of bulk Co_2C presents the similar hexagonal arrangement as hcp Co (0001), with ABAB…stacking of the atomic planes of cobalt. Carbon atoms occupy the octahedral sites in the lattice. The optimized Co–C distance is 1.91 Å. The Co–Co distance in Co_2C is calculated to be 2.62 Å, slightly larger than that in hcp metal Co (2.49 Å). The structure of Co_2C can be treated as interstitial compound of the diffusion of carbon atoms into the cobalt lattices.

Since the Co_2C is formed under the FTS condition, its relative stability could be evaluated by formation heat ΔH_{Co_2C}, as defined below:

$$2Co + CO + H_2 \rightarrow Co_2C + H_2O + \Delta H_{Co_2C} \quad (4)$$

Neglecting the contributions from vibration, the ΔH_{Co_2C} from DFT calculations is −0.81 eV per Co_2C formula. It is clear that under FTS condition, the formation of cobalt carbide is energetically favorable, which agrees well with the experimental observations of the formation of the cobalt carbide [44,53, 55,67,68].

On the other hand, graphite carbon formation has been reported under the reaction conditions [69], and corresponding formation energy $\Delta H_{graphite}$ could be defined as:

$$2Co + CO + H_2 \rightarrow 2Co + C_{graphite} + H_2O + \Delta H_{graphite} \quad (5)$$

The $\Delta H_{graphite}$ is calculated to be −1.18 eV, lower than the formation energy of Co_2C by 0.37 eV with respected to CO and H_2. This indicates that Co_2C is metastable and could decompose to the more stable graphite and metal Co if the kinetic limitations can be overcome. This is inline with experimental observation [45,50]. For comparison, we note that the formation of η-Fe_2C which shares the same space group Pmnn as Co_2C, is strongly exothermic, with the formation energy of −1.01 eV [70] with respect to graphite carbon and iron. This is understandable since the reactivity of Fe is much higher than Co. Indeed, the iron carbide has been thought to be the active phase for the FT synthesis [25,37].

3.2. Electronic properties

To obtain further insights into the interaction between C and cobalt in bulk Co_2C at equilibrium state, we calculated the total density of states (TDOSs) and site-projected partial density of states (PDOSs), which yield the contribution of the *s*-, *p*-, and *d*-states to the TDOSs. The TDOSs of Co_2C at theoretical equilibrium lattice constant are shown in Fig. 2. In this system, there are three distinct regions: the lower lying valence band, the high lying valence band, and the conduction unoccupied band above Fermi level. It can be found that the up and down densities of state of all the three bands are almost symmetric, which means that there is almost no magnetic characteristic of Co_2C. The previous studies have shown that Co_3C is metallic-like and exhibits ferromagnetic states [71].

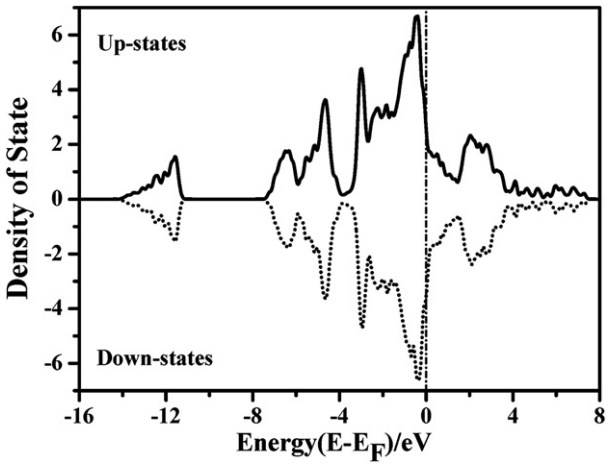

Fig. 2. Calculated total density of states (TDOSs) for Co_2C.

The site-projected partial densities of states (PDOSs) of Co_2C are shown in Fig. 3(PDOSs of Co, see Fig. 3(A); PDOSs of C, see Fig. 3(B)), in which the total densities at each atom as well as the different components (*s*, *p*, and *d*) are shown separately. The lower lying valence band ranging from −14 to −11 eV is composed by an admixture of C 2 *s* states and a small contribution from 4 *s*, 4*p* and 3 *d* states of cobalt. The high lying valence band can be separated into two parts: the first one ranges from −7.5 to about −4 eV and constitutes the hybridization of C 2*p* with small Co 4 *s*, 4*p* and 3 *d* states; the second one, from −4 up to Fermi level, is mainly formed by Co 3 *d*. No energy gap near the Fermi level is found, which indicates the metallic nature of Co_2C. The unoccupied conduction region beyond the Fermi energy is actually resulting from cobalt 3*d* states with only a very small contribution from carbon 2*p* states. The contributions of cobalt 4*s* and 4*p* states to the conduction band are sufficiently small and can be negligible.

Lv et al. [70] and Faraoun et al. [72] explored the TDOSs and PDOSs of η-Fe_2C. According to their calculations, three regions of TDOSs as in Co_2C were found for η-Fe_2C, and the contribution of the total densities at each atom as well as the different components (*s*, *p*, and *d*) to the regions on η-Fe_2C is similar to that on Co_2C. Likewise, no energy gap near the Fermi level is found for η-Fe_2C, which indicates that the material has a similar metallic nature as Co_2C does. However, the electronic structure of η-Fe_2C has a distinct feature from Co_2C. The up and down states of the lower lying valence band is almost symmetric, whereas those near the Fermi level are noticeably dissimilar for η-Fe_2C. Therefore, the calculated magnetic moments were quite different for the two carbides: η-Fe_2C [70] has magnetic characteristic with atom-averaged magnetic moment of 1.09μ_B while the Co_2C has no magnetic characteristic.

To illustrate the chemical bonding property of Co_2C, we also calculate the difference of charge density, as plotted in Fig. 4. We can see immediately that a strong direct bonding exists between Co and C, which suggests a covalent bonding between carbon and cobalt atoms. Furthermore, there is electron depletion around Co atom, and charge accumulation with the distance nearer to carbon, which reveals an ionic contribution between positive charged Co and negative charged C to the bonding. Therefore, our results demonstrate similarly to η-Fe_2C reported in literature that the bonds of Co_2C are also of the unusual mixtures of metallicity, covalence, and ionicity.

3.3. Co_2C surface stability

The surface structures for the considered low index surfaces of Co_2C are depicted in Fig. 5 for (100), (001), (010), Fig. 6 for (101), (011), (110) and Fig. 7 for (111), respectively. The structural and energetic information of bulk-terminated stoichiometric Co_2C surfaces are given in Table 2, including in-plane lattice constants *u* and *v* (Å) and area *A* (Å^2) of surface (1×1) unit cell, calculated surface energy γ (meV/Å^2), differential adsorption energy by removing or adding one surface Co atom with respect to the stoichiometric surface and the interlayer distances *d* (Å) for the outmost atoms. All in-plane lattice vectors (*u* and *v*) of these low index surfaces are orthogonal except (111), in which the angle between *u* and *v* is 72.4°. The calculated coordination numbers of Co and C (noted as N_{Co} and N_C hereafter) in the outmost layer are also shown in Table 2 for comparison.

We focus on the relative stability of the seven stoichiometric surfaces, and later on the results of non-stoichiometric surfaces will be also discussed and analyzed. Note that the surfaces with single-bond dangling terminations are not included here since they are extremely unstable.

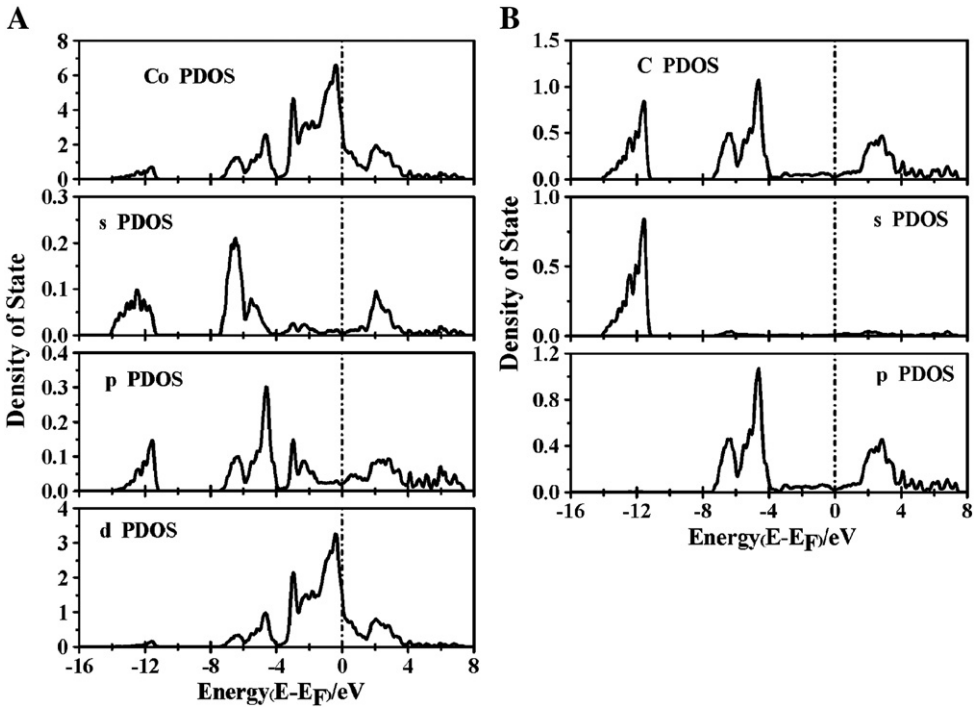

Fig. 3. Calculated site-projected partial densities of states (PDOSs) of Co_2C: (A) Cobalt PDOSs, (B) Carbon PDOSs. The dotted lines are the Fermi level.

3.3.1. (001), (010) and (100) surfaces

The 2D unit cells of (001) and (010) surfaces both have the rectangular geometry (2.88 Å × 4.39 Å and 2.88 Å × 4.35 Å), with similar surface area of 12.64 $Å^2$ and 12.53 $Å^2$, respectively. The complete bulk-like stacking of stoichiometric (001) and (010) surfaces are formed by three consecutive layers, i.e., the local atom arrangement on the *i*-th layer is reestablished in the $(i+3)$-th layer as shown in Fig. 5. The stoichiometric terminations for (001) and (010) surfaces consist of Co on the outmost layer. The coordination number of surface cobalt and carbon atoms is two-fold and five-fold. As listed in Table 2, the surface energy of stoichiometric (001) surface was higher than the stoichiometric (010) surface, with the values of 170 meV/$Å^2$ and 144 meV/$Å^2$ respectively. Since the coordination number of surface carbon and cobalt atoms between (001) and (010) surfaces is same, the difference in surface energies can be attributed to their structural variations. Indeed, we find that the calculated first interlayer distance between negative charged carbon and positive charged cobalt for (001) surface is 0.09 Å larger than that of the (010) surface. This will induce the larger dipole of (001) surface, thereby raises the surface energy accordingly.

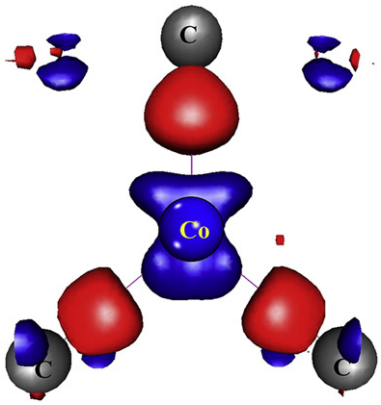

Fig. 4. Calculated difference of charge density of Co_2C. The red and blue colors indicate electron depletion and accumulation, respectively.

The (100) orientation has a quasi-square geometry (4.39 Å × 4.35 Å) with surface area of 19.10 $Å^2$. The stoichiometric (100) surface is mixed with C and Co (noted as $T_{Co/C}$). The calculated first interlayer distance between carbon and cobalt of (100) is only

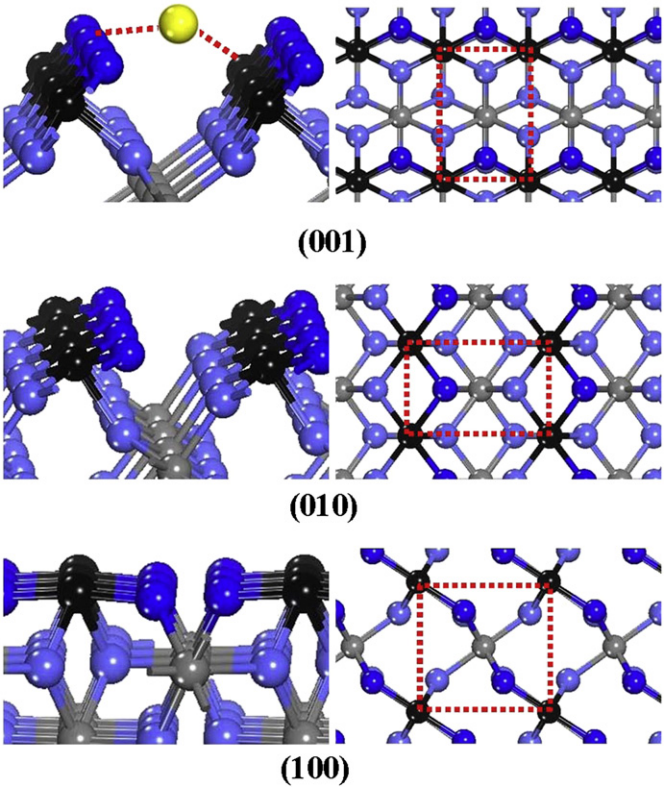

Fig. 5. Schematic views of bulk-terminated stoichiometric (001), (010) and (100) p(1 × 1) surfaces of Co_2C(left: side view, right: top view). The dashed line in the right part represents the surface unit cell. The black and dark bule balls represent C and Co atoms in the outmost layers, respectively; the yellow balls are Co atoms added to the stoichiometric surfaces to obtain non-stoichiometric surfaces.

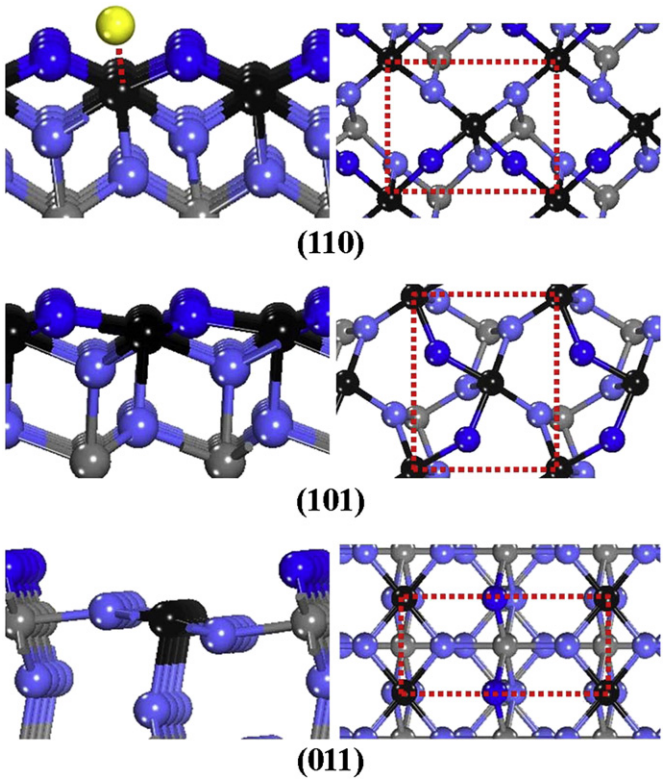

Fig. 6. Schematic views of bulk-terminated stoichiometric (110), (101) and (011) p(1×1) surfaces of Co_2C, left: side view, right: top view. The dashed line in the right part represents the surface unit cell.

0.11 Å, which will induce small dipole, compared to 0.51 Å and 0.42 Å for (001) and (010) surface. Combining with greater surface area than stoichiometric (010), one may expect that the stoichiometric (100) should have higher surface stability. However, the surface energy of stoichiometric (100) surface is higher than the (010) surface by 18 meV/Å^2. The lower surface stability of stoichiometric (100) might originate from the lower coordination number of carbon atoms (four), compared with that on stoichiometric (010) surface (five). This also explains the different surface stability between stoichiometric (100) and (001) surface, with 8 meV/Å^2 difference in surface energy found.

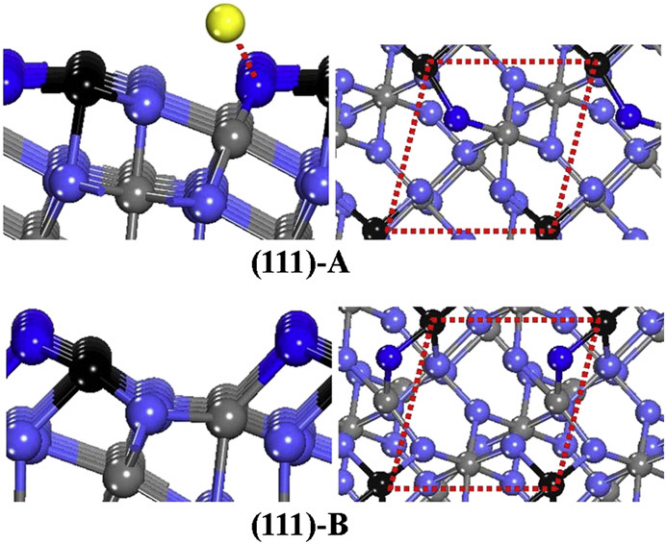

Fig. 7. Schematic views of bulk-terminated stoichiometric (111) surface of Co_2C: (A) type $T_{Co/C}$; (B) type T_{Co}. The dashed line in the right part represents the surface unit cell.

Table 2
Analysis of the surface structures, the surface energy γ (meV/Å^2) of bulk − terminated stoichiometric Co_2C surfaces and the interlayer distances d (Å) for the outmost negative charged carbon and positive charged cobalt atoms. E_{diff}^{stoic} and E_{diff}^{extra} are the differential adsorption energy by removing or adding extra Co atoms with respect to stoichiometric surface as defined in the main context.

Surface	(u, v) (Å)[a] surface area (Å^2)	γ (meV/Å^2) (N_{Co}, N_C)[b]	E_{diff}^{stoic}(eV)	E_{diff}^{extra}(eV)	d(Å)
(001)	(2.88,4.39) 12.64	170 (2, 5)	−0.08	0.02	0.51
(010)	(2.88, 4.35) 12.53	144 (2, 5)	0.36	–	0.42
(100)	(4.39,4.35) 19.10	162 (2, 4)	–	–	0.11
(110)	(4.35,5.25) 22.83	161 (2, 5)	0.26	−0.03	0.61
(101)	(5.22, 4.39) 22.92	129 (2, 5)	0.85	–	0.27
(011)	(2.88, 6.18) 17.57	135 (2 + 3, 5)	−0.28	–	1.11
(111)–A	(5.25,5.22) 27.41	170 (2, 4)	0.77	−0.77	0.07
(111)–B		170 (2, 4)	−0.77	–	0.50

[a] The calculated surface in-plane lattice constants (u, v) (Å) of surface (1×1) unit cell and corresponding surface area in Å^2 are indicated. The lattice vectors are orthogonal for all surfaces except (111), where the angle is 72.4°.
[b] The coordination number of exposed Co and C atoms, N_{Co} and N_C, in the outmost layer are indicated too.

We use Eq. (2) and Eq. (3) to measure the relative stability of the non-stoichiometric (001) and (010) surfaces. The calculated differential adsorption energies for removing surface Co atom or adding extra Co atom are listed in Table 2. With one extra Co atom coordinated to exposed carbon on the stoichiometric (001) surface, the calculated adsorption energy E_{diff}^{extra} is 0.02 eV, which means that this process is energetically unfavorable. On the other hand, we note that the differential adsorption energy by removing Co from the stoichiometric surface is −0.08 eV, indicating that carbon terminated (001) surface is energetically favorable. Therefore, the (001) surface prefers non-stoichiometric carbon-terminated surface and the Co atoms of the surface would tend to aggregate and form small Co nanoparticles on the surfaces. For the stoichiometric (010) surface, the energy cost for removing the surface Co atom is 0.35 eV, implying that the (010) surface prefers stoichiometric Co-terminated surface, which is in line with its lower surface energy.

3.3.2. (110), (101) and (011) surfaces

As seen clearly from Fig. 6, the (110) and (101) surface exhibit similar rectangular structure, with the (4.35 Å×5.25 Å and 4.39 Å×5.22 Å) 2D unit cells respectively. The surface areas per (1×1) unit cell are calculated to be 22.83 Å^2 and 22.92 Å^2. The coordination number for surface C and Co atom on stoichiometric (110) and (101) surfaces are five and two respectively. According to our calculation, the interlayer distance between Co and C layers on stoichiometric (110) is 0.34 Å larger than the stoichiometric (101) surface, which will result in higher dipole. Since the surface areas and coordination number of surface atoms on the (110) and (101) surface are similar, the dipole difference induced by interlayer distance variation can be the main reason for the different surface stability: the stoichiometric (110) surface has a higher surface energy than stoichiometric (101) surface by 32 meV/Å^2 (161 meV/Å^2 versus 129 meV/Å^2).

The (011) surface has a rectangular geometry with a 2.88 Å×6.18 Å 2D unit cell. The (1×1) surface area is 17.57 Å^2 and the calculated surface energy is 135 meV/Å^2. It should be noticed that the dipole difference between stoichiometric (011) surface and (101) surface is even larger than that between (101) surface and (110) surface. As shown in Table 2, the interlayer distance difference for the outmost two layers between stoichiometric (011) surface and (101) surface is 0.84 Å,

which is larger than that between (101) surface and (110) surface by 0.50 Å. It can be expected that this will lead to a large increase in the surface energy. However, the difference of the surface energy between stoichiometric (011) surface and (101) surface is only 6 meV/Å^2. This could be due to the fact that the energy compensation induced by coordination number increase (three-fold and two-fold coordinated Co on (011) surface versus two-fold Co on (101)) compensates the energy cost due to dipole increase of (011) surface energy to a great extent.

We now turn to the stability of non-stoichiometric (110), (101) and (011) surfaces. For stoichiometric (110) and (101), the calculated differential adsorption energies E_{diff}^{stoic} for removing terminated Co are 0.26 eV and 0.85 eV, which means that the new formed Co-poor carbon terminated surfaces are both less favorable than the stoichiometric Co-terminated surfaces. With one extra Co atom coordinated to exposed carbon on stoichiometric (110) surface, the calculated differential adsorption energy (E_{diff}^{extra}) is −0.02 eV, which means that this process is energetically favorable, and the new formed cobalt terminated (Co-rich) surface is more stable than corresponding stoichiometric surface. However, this is not the case for the stoichiometric (011) surface, which has the differential adsorption energy of −0.28 eV for the formation of the mixed Co/C termination (Co-poor) by removing the surface Co atom. This suggests that the new formed Co/C terminated (Co-poor) surface is energetically more preferential than stoichiometric (011) surface, and the (011) surface prefers Co/C terminated non-stoichiometric (Co-poor) configuration. In other word, this indicates again that the Co atoms of the outmost layer would tend to aggregate and form small Co nanoparticles.

3.3.3. (111) surface

Unlike all the other low index stoichiometric surfaces, two possible stoichiometric (111) terminations can be cleaved from bulk Co_2C. The side and top view of the structures of the two stoichiometric surfaces are illustrated in Fig. 7, noted by stoichiometric (111)-A and (111)-B surfaces, respectively. The stoichiometric (111)-A surface is mixed with carbon and cobalt ($T_{Co/C}$), whereas the stoichiometric (111)-B surface is Co terminated (T_{Co}) in the outmost layer. The carbon is four-fold coordinated and the cobalt is two-fold coordinated for the two types of stoichiometric (111) surfaces. The interlayer distances between negative carbon and positive cobalt for stoichiometric (111)-A and (111)-B surfaces are 0.07 Å and 0.50 Å, respectively. The calculated surface energies are shown in Table 2. It can be seen from Table 2 that the two stoichiometric (111) surfaces have the same surface energy of 170 meV/Å^2.

By removing the surface Co atom and adding one Co atom on stoichiometric (111)-A surface, one Co-poor non-stoichiometric surface terminated with carbon (T_C) and one Co-rich non-stoichiometric termination with mixed Co/C ($T_{Co/C}$) are formed. Likewise, one Co-poor non-stoichiometric surface terminated with carbon (T_C) can be obtained from stoichiometric (111)-B by removing the surface Co atom. It is interesting to note that the two new formed non-stoichiometric (111) surfaces terminated with carbon are of different stability. For the non-stoichiometric (111)-A surface, the differential adsorption energy(E_{diff}^{stoic}) is 0.77 eV, which means that the new formed T_C termination is energetically unfavorable than corresponding stoichiometric surface. While the new formed carbon terminated (T_C) non-stoichiometric (111)-B surface is favorable than corresponding stoichiometric surface with the differential adsorption energy(E_{diff}^{stoic}) of −0.77 eV. The coordination number difference and dipole difference are responsible for the stability changes of non-stoichiometric (111) -A terminations. As shown in Table 2, some of the exposed carbon atoms are only three-fold coordinated for the non-stoichiometric T_C (111)-A termination, less than corresponding stoichiometric surface (four-fold). Meanwhile, the interlayer distance between Co and C layers on the non-stoichiometric (111) is 0.21 Å larger than the stoichiometric surface, which further results in higher dipole and hence higher surface energy. While in the case of the carbon-terminated non-stoichiometric (111)-B surface, the coordination number difference is mainly responsible for the stability changes with little contribution of dipole difference. Although part of carbon atoms are three-fold coordinated, less than stoichiometric surface (four-fold), but the cobalt atoms are six-fold coordinated, which leads to much higher stability of the new formed Co-poor surface than corresponding stoichiometric surface with two-fold corrdinated cobalt atoms.

We note that the calculated differential adsorption energy(E_{diff}^{extra}) is −0.77 eV to form the non-stoichiometric $T_{Co/C}$ terminated(Co-rich) surface by adding extra Co on Co/C terminated stoichiometric (111)-A surface, which means that the Co-rich $T_{Co/C}$ termination is much more favorable than the corresponding stoichiometric surface. This can also be understood from the coordination effect, since the coordinate number of surface cobalt (three-fold) and carbon (five-fold) atoms on the $T_{Co/C}$ terminated non-stoichiometric (111)-A surface is more than corresponding stoichiometric surface.

3.3.4. Discussion

It is interesting to compare the stability of low index stoichiometric Co_2C surfaces. As listed in Table 2, of all the low index stoichiometric surfaces examined, it can be found that the (001) and (111) surfaces are the least stable, and the (101) and (011) surfaces are the most stable, with the decreased stability order of (101) > (011) > (010) > (110) > (100) > (001) = (111). The higher stability of the (101) and (011) surfaces with respect to the other low index orientations is in agreement with the previous DFT studies on Fe_2C by Bao et al. [73] Overall, we see that the seven low index stoichiometric Co_2C surfaces can be divided into three categories. The (101), (110) and (011) to be the first category, the (001), (010) and (100) to be the second and the (111) to be the third. The first category has the lowest surface energy, with a crossover point of value between (010) and (110) surface.

We now turn our attention to the reason of the surface stability difference between (010) and (110) surfaces. On one hand, the coordination number of surface atoms per unit surface area on the (110) surface is smaller than (010) surface, which would result in the increase in surface energy; on the other hand, the interlayer distances between the first two layers on (110) surface is 0.19 Å longer than the stoichiometric (010) surface, which cause larger dipole and hence further result in surface energy increasing. As a consequence, the combined effects of the two lead to the surface energy of stoichiometric (110) higher in surface energy than (010) surface by 17 meV/Å^2.

On the basis of the analysis about the stability of the low index surfaces, we arrive at the conclusion that the coordination number of surface atoms per unit surface area and the surface dipole both have great influence on the stability of surfaces: the less the coordination number of surface atoms per unit surface area, the lower the stability; the higher the dipole, the lower the stability. For instance, Co_2C (111) surface having less coordination number of surface atoms per unit surface area (four-fold coordinated C per 27.41 Å^2 for (111) versus five-fold coordinated C 22.92 Å^2 for (101)), is less stable than Co_2C (101) surface; the stability of Co_2C (101) surface is higher than (110) surface due to its lower dipole.

4. Conclusions

In the present article, we have carried out a self-consistent periodic density functional theory (DFT) study on the structural and electronic properties of bulk Co_2C and the stability of low index Co_2C surfaces. We found that the formation of Co_2C is exothermic with the formation energy of −0.81 eV/Co_2C with respect to Co under the presence of syngas (mixture of CO and H_2). While formed Co_2C can be decomposed further to metal Co and graphite carbon with modest energy gain of 0.37 eV/Co_2C. This suggests that Co_2C is only metastable in FTS synthesis, which agrees well with experimental findings. The density of states (DOSs) reveals that the Co_2C is paramagnetic and strong metallic-like. The difference of charge density analysis indicates that the bond of

Co_2C is of the mixtures of metallic, covalent, and ionic properties. A variety of low index Co_2C surfaces with different terminations are studied. We find that surface energy highly relies on the surface areas, the coordination number of surface atoms and the surface dipole. The low index stoichiometric surfaces have the decreased stability order of (101) > (011) > (010) > (110) > (100) > (001) = (111). Our results indicate that under Co-poor condition, the formation of non-stoichiometric surface (011) and (111) without terminated cobalt are energetically more favorable, while under Co-rich condition the formation of non-stoichiometric (111) surface with cobalt overlayer is preferential. The role of formation of these non-stoichiometric cobalt carbide surfaces for the high alcohol selectivity found by experiment [55] is under study.

Acknowledgements

We thank the finical supports by the Natural Foundation of Science of China (Grants 20873142, 20733008, 20923001). We appreciate the fruitful discussions with Prof. Yunjie Ding.

Appendix A. Supplementary data

Supplementary data to this article can be found online at doi:10.1016/j.susc.2011.11.025.

References

[1] L.E. Toth, Transition Metal Carbides and Nitrides; Refractory Materials, Academic Press, New York, 1971.
[2] J.G. Chen, Chem. Rev. 96 (1996) 1477.
[3] S.T. Oyama, Catal. Today 15 (1992) 179.
[4] H.H. Hwu, J.G. Chen, Chem. Rev. 105 (2005) 185.
[5] S.T. Oyama, The Chemistry of Transition Metal Carbides and Nitrides, Blakie Academia and Professional, Glasgow, 1996.
[6] S.T. Oyama, G.L. Haller, in: G.C. Bond, G. Webb (Eds.), Catalysis (Specialist Periodical Reports), Vol. 5, Royal Society of Chemistry, London, 1982, p. 333.
[7] V.A.I., A.L. Gubanov, V.P. Zhukov, Electronic Structure of Refractory Carbides and Nitrides, Cambridge University Press, Cambridge, 1994.
[8] J.G. Chen, J. Eng, S.P. Kelty, Catal. Today 43 (1998) 147.
[9] A.T. Santhanam, in: S.T. Oyama (Ed.), The Chemistry of Transition Metal Carbides and Nitrides, Blackie Academic and Professional, Glasgow, 1996, p. 28.
[10] R.L. Levy, M. Boudart, Science 181 (1973) 547.
[11] M.L. Frauwallner, F. Lopez-Linares, J. Lara-Romero, C.E. Scott, V. Ali, E. Hernandez, P. Pereira-Almao, Appl. Catal., A 394 (2011) 62.
[12] M. Espinoza, J. Cruz-Reyes, M. Del Valle-Granados, E. Flores-Aquino, M. Avalos-Borja, S. Fuentes-Moyado, Catal. Lett. 120 (2008) 137.
[13] Y.F. Zhao, A.C. Dillon, Y.H. Kim, M.J. Heben, S.B. Zhang, Chem. Phys. Lett. 425 (2006) 273.
[14] C. Moreno-Castilla, M.A. Alvarez-Merino, F. Carrasco-Marin, J.L.G. Fierro, Langmuir 17 (2001) 1752.
[15] T.J. Zhou, A.M. Liu, Y.R. Mo, H.B. Zhang, J. Phys. Chem. A 104 (2000) 4505.
[16] C.S. Song, W.L. Wang, B.L. Wei, S.T. Oyama, Abstr. Pap. Am. Chem. Soc. 225 (2003) U856.
[17] W. Seidy, W.K. Shiflett, Abstr. Pap. Am. Chem. Soc. 186 (1983) 77-INDE.
[18] N. Lohitharn, J.G. Goodwin, E. Lotero, J. Catal. 255 (2008) 104.
[19] Y.G. Wang, B.H. Davis, Appl. Catal., A 180 (1999) 277.
[20] R.W. Joyner, G.R. Darling, J.B. Pendry, Surf. Sci. 205 (1988) 513.
[21] H. Schaferstahl, Erdol, Kohle, Erdgas, Petrochem. 34 (1981) 31.
[22] S. Weller, L.J.E. Hofer, R.B. Anderson, J. Am. Chem. Soc. 70 (1948) 799.
[23] L.I. Johansson, Surf. Sci. Rep. 21 (1995) 179.
[24] J.J.C. Geerlings, M.C. Zonnevylle, C.P.M. de Groot, Surf. Sci. 241 (1991) 302.
[25] W.C. Chiou, E.A. Carter, Surf. Sci. 530 (2003) 88.
[26] X.Q. Gong, R. Raval, P. Hu, Mol. Phys. 102 (2004) 993.
[27] X.Q. Gong, R. Raval, P. Hu, J. Chem. Phys. 122 (2005) 024711.
[28] Q. Ge, M. Neurock, J. Phys. Chem. C 110 (2006) 15368.
[29] D.B. Cao, S.G. Wang, Y.W. Li, H. Wang, H. Jiao, J. Mol. Catal. A: Chem. 272 (2007) 275.
[30] C.F. Huo, J. Ren, Y.W. Li, J. Wang, H. Jiao, J. Catal. 249 (2007) 174.
[31] X.Y. Liao, D.B. Cao, S.G. Wang, Z.Y. Ma, Y.W. Li, J. Wang, H. Jiao, J. Mol. Catal. A: Chem. 269 (2007) 169.
[32] S. Pick, Surf. Sci. 601 (2007) 5571.
[33] J. Cheng, P. Hu, P. Ellis, S. French, G. Kelly, C.M. Lok, J. Phys. Chem. C 112 (2008) 9464.
[34] J. Cheng, P. Hu, P. Ellis, S. French, G. Kelly, C.M. Lok, J. Phys. Chem. C 112 (2008) 6082.
[35] J. Cheng, X.Q. Gong, P. Hu, C.M. Lok, P. Ellis, S. French, J. Catal. 254 (2008) 285.
[36] C.F. Huo, Y.W. Li, J. Wang, H. Jiao, J. Phys. Chem. C 112 (2008) 14108.
[37] P.J. Steynberg, J.A. van den Berg, W.J. van Rensburg, J. Phys. Condens. Matter 20 (2008) 064238.
[38] J.M. Gracia, F.F. Prinsloo, J.W. Niemantsverdriet, Catal. Lett. 133 (2009) 257.
[39] T. Yang, X.D. Wen, C.F. Huo, Y.W. Li, J. Wang, H. Jiao, J. Mol. Catal. A: Chem. 302 (2009) 129.
[40] E. van Steen, P. van Helden, J. Phys, Chem. C 114 (2010) 5932.
[41] D.B. Cao, Y.W. Li, J. Wang, H. Jiao, J. Mol. Catal. A: Chem. 346 (2011) 55.
[42] D.C. Sorescu, Surf. Sci. 605 (2011) 401.
[43] Y.H. Zhao, K. Sun, X. Ma, J. Liu, D. Sun, H.Y. Su, W.X. Li, Angew. Chem. Int. Ed. 50 (2011) 5335.
[44] J. Xiong, Y. Ding, T. Wang, L. Yan, Catal. Lett. 102 (2005) 265.
[45] O. Ducreux, J. Lynch, B. Rebours, M. Roy, P. Chaumette, Natural Gas Conversion V, 119, 1998, p. 125.
[46] F. Tihay, A.C. Roger, A. Kiennemann, G. Pourroy, Catal. Today 58 (2000) 263.
[47] F. Tihay, G. Pourroy, M. Richard-Plouet, A.C. Roger, A. Kiennemann, Appl. Catal., A 206 (2001) 29.
[48] J. Cheng, P. Hu, P. Ellis, S. French, G. Kelly, C.M. Lok, J. Phys. Chem. C 114 (2010) 1085.
[49] G. Bian, T. Nanba, N. Koizumi, M. Yamada, J. Mol. Catal. A: Chem. 178 (2002) 219.
[50] O. Ducreux, B. Rebours, J. Lynch, M. Roy-Auberger, D. Bazin, Oil & Gas Science and Technology-Revue De L Institut Francais Du Petrole 64 (2009) 49.
[51] J. Llorca, N. Homs, J. Sales, P.R. de la Piscina, J. Catal. 209 (2002) 306.
[52] M.L. Xiang, D.B. Li, W.H. Li, B. Zhong, Y.H. Sun, Catal. Commun. 8 (2007) 503.
[53] G.G. Volkova, T.M. Yurieva, L.M. Plyasova, M.I. Naumova, V.I. Zaikovskii, J. Mol. Catal. A: Chem. 158 (2000) 389.
[54] X.D. Xu, J.J.F. Scholten, D. Mausbeck, Appl. Catal., A 82 (1992) 91.
[55] G.P. Jiao, Y.J. Ding, H.J. Zhu, X.M. Li, J.W. Li, R.H. Lin, W.D. Dong, L.F. Gong, Y.P. Pei, Y. Lu, Appl. Catal., A 364 (2009) 137.
[56] N. Seriani, F. Mittendorfer, G. Kresse, J. Chem. Phys. 132 (2010) 024711.
[57] P. Sautet, F. Cinquini, ChemCatChem 2 (2010) 636.
[58] F. Abild-Pedersen, O. Lytken, J. Engbaek, G. Nielsen, I. Chorkendorff, J.K. Norskov, Surf. Sci. 590 (2005) 127.
[59] M. Marsman, G. Kresse, J. Chem. Phys. 125 (2006) 104101.
[60] G. Kresse, J. Furthmuller, Phys. Rev. B 54 (1996) 11169.
[61] J.P. Perdew, J.A. Chevary, S.H. Vosko, K.A. Jackson, M.R. Pederson, D.J. Singh, C. Fiolhais, Phys. Rev. B 46 (1992) 6671.
[62] Y. Wang, J.P. Perdew, Phys. Rev. B 44 (1991) 13298.
[63] P.E. Blöchl, Phys. Rev. B 50 (1994) 17953.
[64] G. Kresse, D. Joubert, Phys. Rev. B 59 (1999) 1758.
[65] H.J. Monkhorst, J.D. Pack, Phys. Rev. B 13 (1976) 5188.
[66] J. Clarke, K.H. Jack, Chem. Ind., London, (1951) 1004.
[67] P.A. Premkumar, A. Turchanin, N. Bahlawane, Chem. Mater. 19 (2007) 6206.
[68] Y.H. Lee, Y.S. Huang, J.F. Min, G.M. Wu, L. Horng, J. Magn. Magn. Mater. 310 (2007) 913.
[69] K.F. Tan, J. Xu, J. Chang, A. Borgna, M. Saeys, J. Catal. 274 (2010) 121.
[70] Z.Q. Lv, S.H. Sun, P. Jiang, B.Z. Wang, W.T. Fu, Comput. Mater. Sci. 42 (2008) 692.
[71] I.R. Shein, N.I. Medvedeva, A.L. Ivanovskii, Physica B 371 (2006) 126.
[72] H.I. Faraoun, Y.D. Zhang, C. Esling, H. Aourag, J. Appl. Phys. 99 (2006) 093508.
[73] L.L. Bao, C.F. Huo, C.M. Deng, Y.W. Li, J. Fuel Chem. Tech. 37 (2009) 104.